# Topographic swath profile analysis: a generalization and sensitivity evaluation of a digital terrain analysis tool

Tamás Telbisz, Gábor Kovács, Balázs Székely, and Judit Szabó

with 13 figures and 3 tables

**Summary.** Swath profile analysis is considered to be an improved, DTM-based version of traditional cross-section analysis. To avoid arbitrariness of simple line profiles, the swath method horizontally expands the cross-section line into a rectangular swath. Commonly, profile Z values are calculated as statistical parameters (minimum, mean, maximum, etc.) of elevation values being at the same distance from the baseline of the swath. Swath profile analysis proved to be useful in the study of large orogens to evaluate the effects of vertical surface movements as well as in the investigation of fluvially or glacially sculpted topography. However, there is still a lack of a summarized methodological description that this paper aims to make up for, additionally presenting a brief review of earlier swath-based studies. Although previous studies used the term swath for rectangular units only, we, generalizing its possible usage, extend this analysis to circular and curvilinear polygons as well so that it can be useful in the topographic characterization of volcanoes or large, curved orogens.

In order to demonstrate the usefulness and applicability of swath profiles, the method is tested on an artificial surface, first. Secondly, swath profile analysis is applied to a hilly terrain in the Eastern Alpine Foreland, the Western Pannonian Alpine Foothills. This analysis helped to identify topographic rims, tilted remnant surfaces and fluvial incision within the study area, even where these features are obscured by the dissected topography. Using this area as an example, sensitivity to swath width, swath orientation and swath horizontal resolution was assessed in terms of comparison diagrams and numerical statistics (RMSE, tilt and step parameters). As a result, it is concluded that swath profiles and quantitative landform parameters are found in an acceptably narrow range for relatively large changes in width, azimuth and swath resolution that supports the intuitive application of this method.

*Key words:* circular swath, curvilinear swath, DTM, tectonic geomorphology, Eastern Alpine Foreland

## 1    Introduction

Geomorphological analyses frequently require the reconstructions of remnant surfaces, which are preserved as ridge lines. In other cases, morphological features such as terraces or large-scale slopes or peak elevations are to be presented by elevation profiles but it is difficult to select a single profile which would show all of these features. Furthermore, in tectonic studies, there is often a need to depict and measure the maximum and/or average height of different structural units. In all of the above situations, topographic swath profile analysis can be a useful tool.

Graphical representation of elevation cross-sections is one of the most traditional methods in geomorphology and in many other earth sciences as well. However, the selection of a given cross-section line is always subjective, sometimes resulting in somewhat random pattern or quite the contrary, biased, or too tendentious. In order to avoid this problem, more profiles can be examined jointly: the elevations are measured along parallel and equidistant lines and the profiles are presented in the same diagram. This method is mentioned as "projected profiles" or "topographic swath profile" by Baulig (1926) and by Tricart & Cailleux (1957) (both cited in Grohmann 2011). This could help in identifying characteristic or peak levels in the topography, but the inclusion of too many profiles may result in a "chaotic", unclear graph.

Another solution to avoid problems due to the subjective nature of cross-sections is the topographic swath profile analysis in its modern form. This is a quantitative terrain analysis tool that was realizable only after digital elevation models (DEMs) became widely available. Since the beginning of 1990s several authors used this method (e. g. Fielding et al. 1994 and references later on), however, a general methodological overview seems to be still lacking in the literature.

The aim of this study is to briefly review the use of this method in previous publications, to give a definition of the method, to extend this definition for special cases (curvilinear and circular swaths), to present simple signals in the swath by the example of an artificial test surface and to examine swath sensitivity to the most important parameters (width, orientation, horizontal resolution) by the application example of a hilly landscape found in the Eastern Alpine Foreland in western Hungary and eastern Austria.

## 2    *What is it for? – A brief review of swath analysis studies*

### 2.1    *Classic applications of swath analysis*

Swath analysis is most widely used in tectonic geomorphology. Numerical evaluation of tectonic uplift or subsidence, detection of fault location, explanation of river capture and antecedent valley formation as well as testing of geophysical models are among the most common applications. Most of these papers focus on large-scale, active, orogenic belts (Himalaya, Andes, European Alps, Southern Alps of New Zealand). One of the pioneering works, that of Fielding (1996) uses large-scale swath profiles to compare magnitudes (height, width) of the largest orogenic belts, namely the Tibetan plateau, Altiplano, Alps and Southern Alps (NZ). The relationship of erosion, precipitation and tectonic uplift was studied by Thiede et al. (2004), Bookhagen et al. (2005), Hoke et al. (2005) and Champagnac et al. (2009) using in some cases precipitation swath profiles as well. In high mountain environments, glacial erosion is of outstanding importance leaving characteristic prints on swath profiles (e. g. equilibrium line altitude /ELA/, cirque valley incision, etc.) as it is demonstrated by Bishop et al. (2003), Munroe (2006) and Van der Beek & Bourbon (2008). Foster et al. (2008) studied the glacial buzzsaw hypothesis by the example of the northern Basin and Range (USA). Kühni & Pfiffner (2001) used swath profiles to study the impact of rock erodibility on mountainous relief. Topographic asymmetry can be also assessed with the help of swath profiles (e. g. Musumeci et al. 2003, Dortch et al. 2011). Fluvial erosional effects (e. g. drainage reorganization, terrace

locations) were examined in terms of swath analysis by Pratt-Sitaula et al. (2004), Korup et al. (2005), Rehak et al. (2008), Robl et al. (2008), Godard et al. (2009), Stüwe et al. (2009) and Wegmann & Pazzaglia (2009). Swath analysis method can be useful to recognize denudation steps in topography (Grohmann 2004). Recently, uplift and erosion were extensively studied by dynamic surface process modeling. In some of these studies, the resulted model surfaces were also examined by swath analysis methods (Hoke & Garzione 2008, Johnson et al. 2009, Stüwe et al. 2009). The dynamic equilibrium of uplift and erosion may lead to steady state topography. Swath analysis was used to test the existence of steady state by e.g. Pratt-Sitaula et al. (2004), Thiede et al. (2004) and Stolar et al. (2007).

The maximum values in swath profiles are often interpreted as preserved paleo-surface levels (plateaus, ridges, or in case of volcanic geomorphology planèzes/triangular facets). In certain settings, these paleo-surfaces can be theoretically reconstructed from these remnant parts, and then incision rate or the volume of eroded material can be calculated. Telbisz (2011) studied remnant surfaces of karst topography using swath profiles. Karátson et al. (2012) created circular swath profiles (for definition of this notion see the next section) about Andean volcanoes. Another, very different application is presented by Houser & Mathew (2011), who used swath analysis to study alongshore variations in coastal dune development.

## 2.2  *Scale and scope of swath analysis applications*

In the set of the above mentioned papers, the most widely used DEM was the SRTM database, with horizontal resolution of 3″ (~ 90 m) for most part of the Earth and 1″ (~ 30 m) for the territory of the USA (Rabus et al. 2003). However, earlier publications or very large area studies used occasionally lower resolution DEMs (e.g. Godard et al. 2009: GTOPO30, ~ 1 km horizontal resolution). The other end of resolution spectrum is represented by LiDAR-based swath analysis, though at present in a limited (but certainly growing) number (e.g. Staley et al. 2006, Houser & Mathew 2011).

Similarly, the swath length and width are also variable. In the analysis of large orogens, length is typically 500–1,500 km (e.g. Fielding 1996), whereas width is in the order of 10–100 km. Smaller-scale studies (e.g. Staley et al. 2006) use 500–1,000 m length and proportionally smaller width.

## 3  *Definition of topographic swath profile analysis and its methodology*

Although it is considered to be quite straightforward to carry out swath analysis (see references in Section 2), in some cases the actual computation depends on some methodological decisions and details that are often omitted from descriptions. These missing details often hamper comparisons, therefore we consider it necessary to set up a well-defined methodological framework for the sake of clarity. Although swath analysis is also used for other types of data like derivatives of elevation (e.g., relief, slope, aspect, curvature) or any other numeric grids (e.g. precipitation, temperature, etc.), in the following we consider elevation data as input.

Briefly, topographic swath profile analysis can be considered as a generalized cross-section. Instead of simply measuring elevation values along a given, often some-
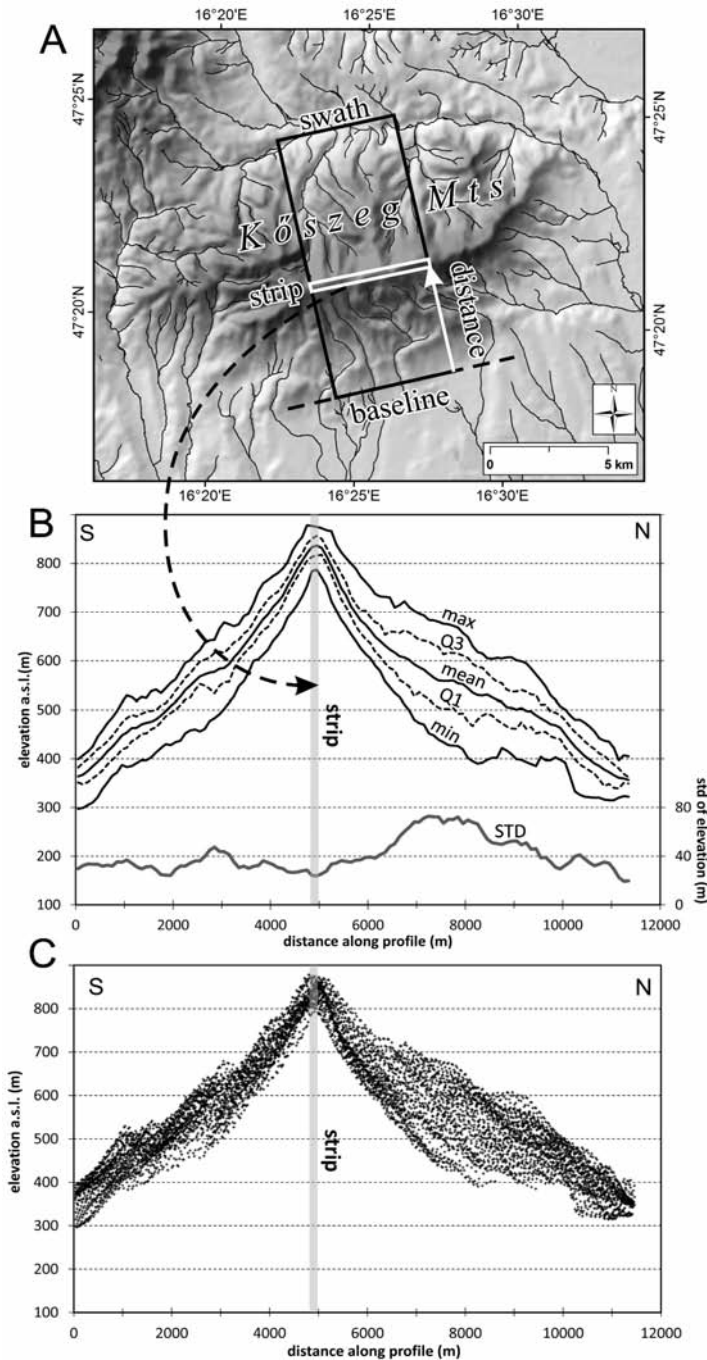
Fig. 1.    Scheme of swath profile construction. A: SRTM3 DTM of the Kőszeg Mts. (for loca-
tion see Fig. 7); B: Swath profile of the sample area (Q1: lower quartile, Q3: upper quartile,
STD: standard deviation); C: Point elevation vs. baseline-distance data of the sample area.

what arbitrary line, in swath analysis all the elevation values within a strip rectangular to the main orientation of the swath are taken into account. Then this elevation data set is used to calculate statistical variables that reveal the specific characteristics of the topography that cannot be mapped with one single profile. As for the visualisation of the swath, these values are plotted as a function of distance from the swath-baseline along the swath (fig. 1). As the rectangular swath is the most common layout of swath analysis, the next section considers this setting for the sake of a clear definition. Later on we extend the meaning of the swath construction to other geometrical shapes analogously to the classic rectangular swath analysis.

## 3.1   *Rectangular swath*

Technically speaking, to carry out a classic swath analysis starting from the DEM, the following steps are necessary:
1) Definition of the investigation swath (usually a rectangle) from the DEM. One side of the swath is defined as baseline.
2) For each point within the swath, distance from baseline is calculated.
3) Points are binned into strips according to their baseline distance.
4) For each bin, statistical parameters of elevation values are calculated (most typically minimum, maximum and mean, as well as range for the relief, but standard deviation, median, quartile and other parameters are also possible).
5) Selected statistical parameters are plotted against the distance to the baseline (fig. 1b).

By omitting Steps 3 and 4 there is a possibility to create a scatter-plot diagram from all elevation values within the swath as a function of baseline distance (fig. 1c). Occasionally, this process may produce a well interpretable figure, but more typically, the resulted scatter-plot is too dense for visual interpretation.

In the framework of swath analysis, several statistical parameters can be calculated beside mean, minimum and maximum elevations. Range is the most widely used parameter, which is in a geomorphological context the same as local relief (i.e. maximum elevation difference) within the strip. Here we note that it is possible to get the local relief swath profile the other way round: calculating a local relief grid first, then creating a mean swath profile using this grid, would also result a local relief swath profile. However, it is somewhat different from the one that is calculated simply by using statistical range in Step 4, because the previous process uses the elevation difference within a given radius circle, whereas the latter process calculates the elevation difference within a strip orthogonal to the swath direction.

It is to be emphasized that the adjustment of swath orientation is an important initial step. It is usually set to be perpendicular to or parallel with the strike of the main geomorphic units, depending on the purpose of the analysis and the statistical variable to be used. The swath width may also influence the resulted profile and the interpretation. It is usually recommended to define swath boundaries so that the selected swath area covers most part of the investigated region but at the same time leaving out those parts, which belong to different geomorphic units. A third parameter is the horizontal resolution of the swath that is the bin size (strip width) in Step 3.
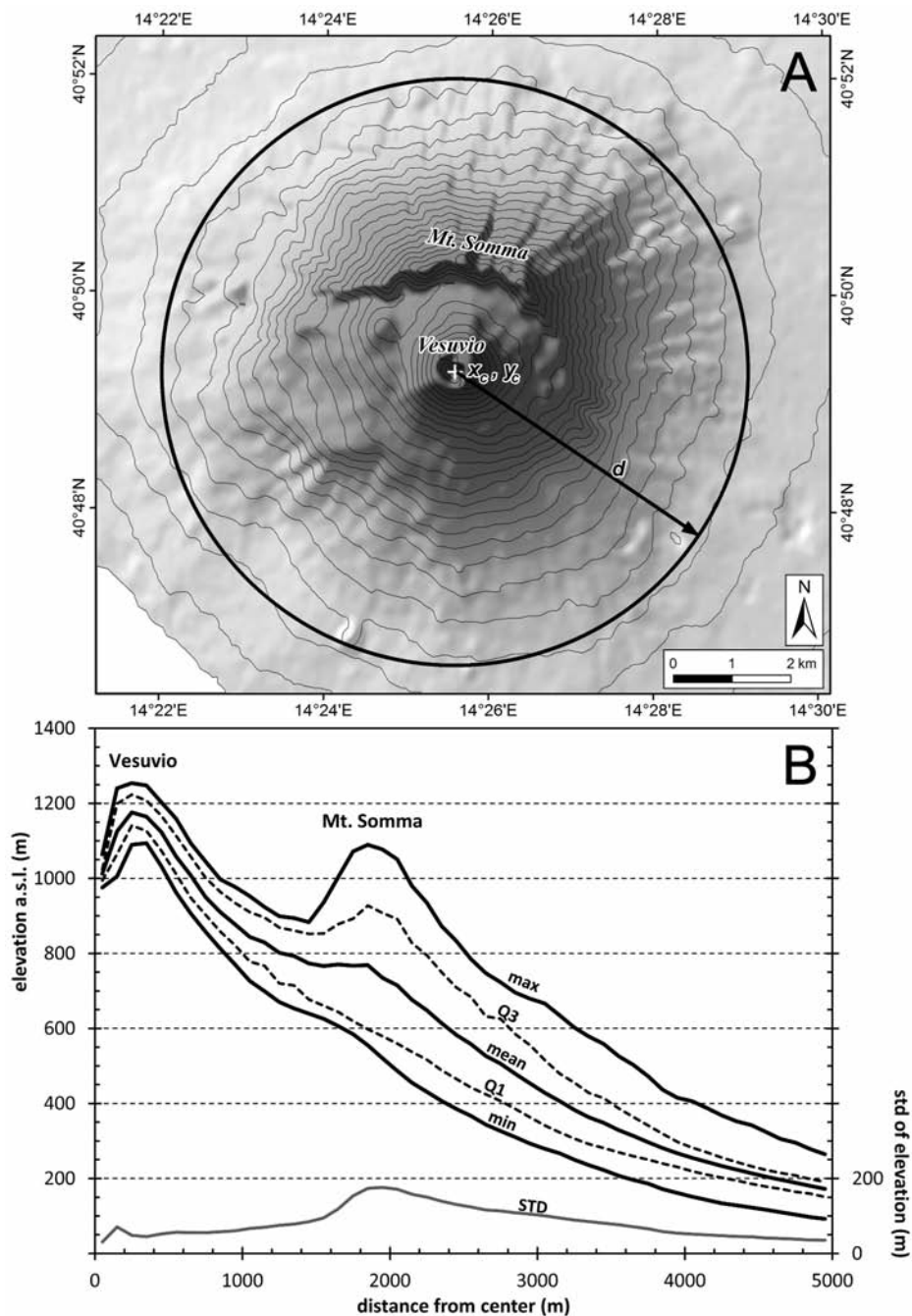
Fig. 2.   Scheme of circular swath profile construction. A: SRTM3 DTM of Mt. Vesuvio; B: Circular swath profile. Note that the Somma caldera is present in the max, Q3, mean and STD curve, but it is not observed in the Q1 and minimum curve, because the caldera is buried in the southern sector.

## 3.2   *Circular swath*

For certain landforms with total or partial circular symmetry it may be useful to consider this generalized form of swath analysis. In this case, a full circle or a pie slice is selected from the DEM and distance can be calculated from the circle (pie) centre point. This layout can be termed as "circular swath". An example is shown for Mt. Vesuvio in fig. 2. In case of circular swaths, the statistical properties of the central part (close to the projection centre) are determined by very few data, while along the outer radii, the number of included points strongly increases. Since the statistical properties are considerably modified by the increasing number of points, this behaviour should be taken into account in the evaluation of circular swath results. This technique of circular swaths is used by Staley et al. (2006) for alluvial fans and by Karátson et al. (2012) for volcanoes, though this term was not used explicitly by these authors.

## 3.3   *Curvilinear swath*

A further different swath arrangement is feasible when along-strike topographic variations are studied for large orogens or mountain chains; as an example, we present here an analysis of the Appalachian Mts. In most cases, the strike is not perfectly linear, therefore the simple distance calculation, as presented in the general case, is not satisfactory. Then, distance calculation and sampling strategy should be redefined. This case can be named as "curvilinear swath" and we do not know of any occurrence in this form in the literature.

The calculation needs the following steps:

1) The swath midline is defined first (e. g. along the main ridge of the mountain chain, or in case of a basin analysis along the trunk channel) and the swath boundary is delimited (e. g. based on the slope map or as a buffer zone around the midline).
2) The midline is represented by an equidistant point set and along profile distances for these points are calculated along the midline.
3) Other DEM pixels within the swath can be assigned to the midline points based on two principles (fig. 3): a) Each pixel is assigned to the closest midline point. It results in a Thiessen-polygon distribution of the swath area. Although in this case, all points are included in the calculations, the Thiessen-polygons can be highly asymmetric to the midline, especially at locations where midline curvature is high; therefore the implying artifacts can be serious. b) The DEM is sampled at equidistant points along lines orthogonal to the midline. (This sampling geometry is similar to the transverse profiles used by Lin & Oguchi 2006, but they studied simple topographic profile shapes, while we use it to derive the swath profile). In this case, a number of pixels are missing from the data evaluation; moreover, at the convex side of the swath, the sampling lines may cross each other, thus the procedure results in an oversampling at these places. On the other hand, larger terrain pieces remain intact by these lines at the concave side that implies undersampling. However, since this sampling is symmetric (as far as the midline is near the center of the swath), the artefacts are less significant than in case 3a, so the second option (3b) is preferred for curvilinear swath profile creation, thus it was applied for the Appalachian swath example (fig. 4).
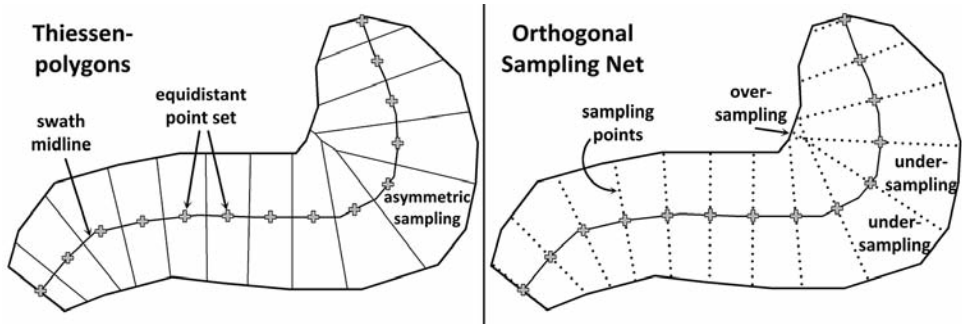
Fig. 3.    Sampling strategies for curvilinear swath construction.
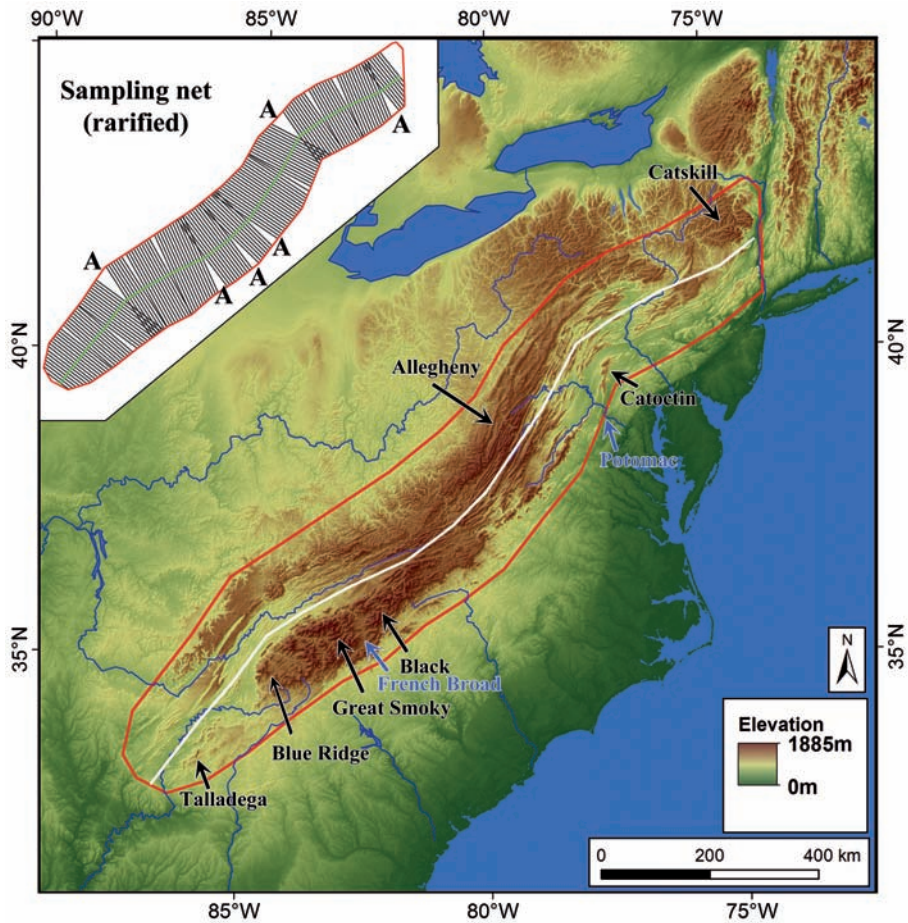


Fig. 4.    Curvilinear swath of the Appalachian Mts. Red polygon: swath boundary; White line: swath midline; inset drawing shows the midline-orthogonal sampling net (rarified for the sake of visibility); 'A' marks artefact location due to biased sampling; DTM is the SRTM30.

4) For each midline sample point, statistical parameters of elevation values are calcu-
   lated based on all pixels assigned to this point.
5) Selected statistical parameters are plotted against distance along midline.

The resulting swath profile of the Appalachian example (fig. 5) shows a concise
summary of Appalachian topography with easily identifiable higher mountains
(Great Smoky Mts., Black Mts., Alleghany) and minor topographic changes (e. g. the
step in the lower quartile curve caused by Catoctin Mts.). Note the remarkable local
minimum at French Broad River. However, the Appalachians are presented here as a
methodological illustration only and detailed analysis of this example is not among
the aims of this study. As for the artefacts due to biased sampling, we note that all
turning points are detectable in the swath profile, most clearly as local extremes in the
maximum curve, but less obviously, these are observable in most other curves as well.

### 3.4 *Methodology for swath sensitivity analysis*

Swath sensitivity to orientation, width and horizontal resolution is carefully exam-
ined later on in this paper by the example of the Western Pannonian Alpine Foothills.
    In order to test swath sensitivity to width, swath profiles were repeatedly cre-
ated from rectangles having the same midline but incrementally growing width (1, 4,
7, 10, 13, 16 km). For orientation sensitivity testing the original swath was rotated
around its centre point by different angles (–10°, –5°, 5° and 10°). This implies that
while the central parts of the swaths more or less overlap each other, the northern and
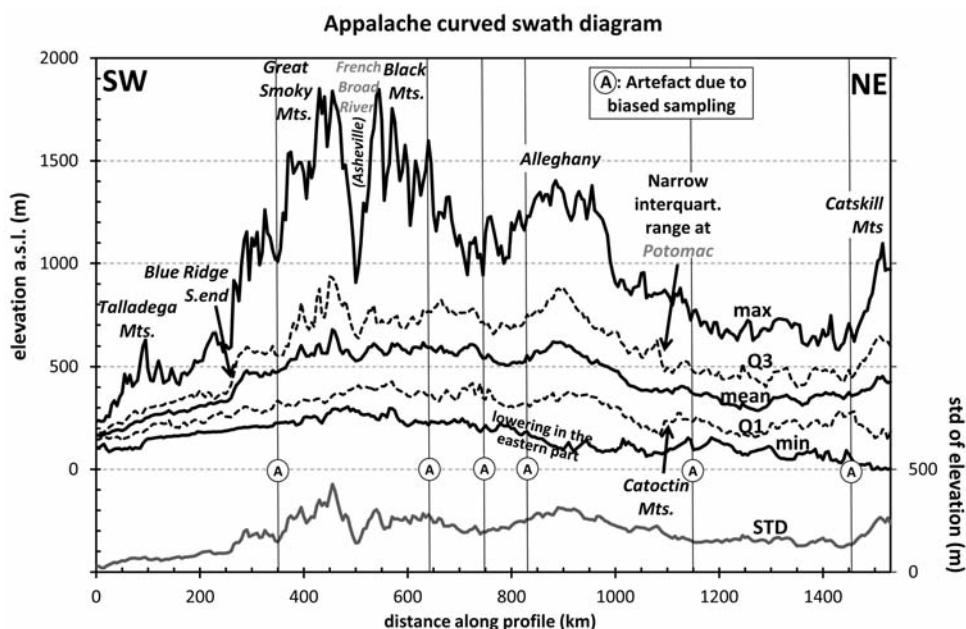


Fig. 5.   Curvilinear swath profile of the Appalachian Mts.

southern parts are almost disjoint for the end members. For bin size sensitivity testing, the profiles were calculated using four different bin sizes (100, 200, 500 and 1,000 m).

Basically, the resulted mean and maximum curves were compared, as well as the standard deviation (STD) curves, which express relief dissection. Further on, standard error of the mean (SEM, the standard deviation divided by the square root of the sample size) was also calculated for each point in the swath profiles to quantify the statistical reliability of the mean curves.

First, the results were evaluated visually based on comparison diagrams. Second, the profiles were compared using the root mean square error (RMSE) and the normalized RMSE (the RMSE divided by the range), too. Third, as the Western Pannonian Alpine Foothills study area contains tilting surfaces and north-facing topographic steps, the profiles were compared specifically, namely how tilt and step height and position values are altered by the changing swaths. North-facing steps were defined as segments between a local minimum and the consecutive local maximum. The position, length and height of these steps were automatically detected and values larger than a given threshold were taken into consideration. Tilt angles were determined uniformly for all curves based on selected segments.

The effect of grid resolution on terrain derivatives were examined by a number of studies (e. g. Zhang et al. 1999, Kienzle 2004). Basically the same constrains are valid for swath profiles if the bin size is changed. Therefore the sensitivity to this parameter is only shortly presented in this study for the sake of completeness.

## 4    Results of swath profile analysis testing

### 4.1    Artificial test surface evaluation

In order to demonstrate how simple landforms influence the swath profile, an artificial test surface was created. Surface tilt was set to 10°, and 200 m wide and 100 m deep, V-profiled river valleys were added as well as a subsided basin surrounded by a 50 m high fault scarp (fig. 6). Four swath rectangles oriented parallel with tilt were analyzed. In swath *A*, *Riv1* crosses the rectangle at an angle slightly different from orthogonal. The resulted signal in profile *A* shows that the maximum curve preserves well the original (pre-incision) surface. This is true for *B*, *C* and '*All*' profiles as well. Since valley direction is almost rectangular to swath *A*, the resulted signal is well-defined, and amplitudes are higher towards the minimum curve. The maximum of STD is found at the northern valley-side, where both the original surface tilt and valley incision contributes to the increased relief.

In swath *B*, both *Riv1* and *Riv2* are oblique to the swath rectangle. *Riv1*'s inflow point is located farther away from the baseline than *Riv2*'s outflow point. As a consequence, the resulted signals of *Riv1* and *Riv2* in swath profile B are stretched and mixed. A common original surface and a common valley bottom level are identifiable in the maximum and minimum curves, respectively. But the unique signals of the rivers are only faintly observable in the quartiles, mean and STD curves.

In swath *C*, where the almost swath-parallel *Riv3* flows into the almost swath-orthogonal *Riv2*, as it was expected, the swath-parallel valley bottom determines a long section of the minimum curve, while the maximum is still preserved at the orig-
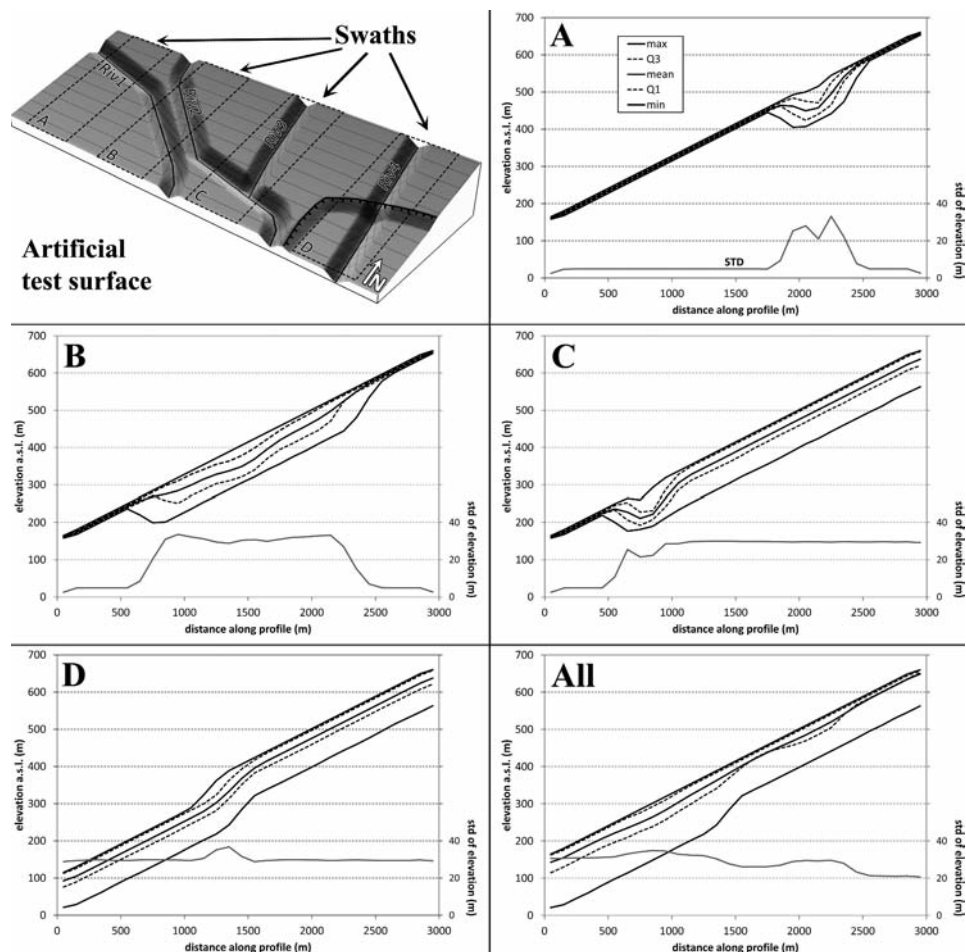
Fig. 6. Artificial surface testing. A, B, C, D are swath profiles based on swath rectangles as shown in the upper-left DEM; 'All' is the swath profile of the whole test surface.

inal surface level. This behaviour demonstrates the power of this technique in separating the effects of paleosurfaces from that of incised forms. The STD is at a continuously high level down to *Riv3* mouth since valley bottom and the original surface are all found within the swath width.

Swath *D* contains an envisioned tectonic depression. The topographic expression of the fault is clearly seen in all curves of profile *D*, that is the maximum curve also has a step and the original surface is not preserved here. In other words, a significant tectonic influence is observable in all the curves and it is clearly distinguishable from incision effects. The along profile distance of this step slightly increases towards the minimum curve that is due to the fact that the fault direction slightly deviates from the swath-orthogonal. STD is almost constant, but the fault step results in an unequivocal increase of this value.

Finally, the swath profile of the whole test surface ('*All*') presents the compound effects of these landforms. The original surface is preserved by the maximum. The quasi-orthogonal section of *Riv1* is reflected in the lower quartile (Q1) and in the STD curves, similarly, the quasi-orthogonal section of *Riv2* is detectable in the STD curve and very faintly in the upper quartile (Q3) and mean curve. The fault step is clearly identifiable in the Q1, minimum and STD curve.

### 4.2   *Swath sensitivity analysis by the example of the Western Pannonian Alpine Foothills*

In order to present further strength of the method and to perform a sensitivity analysis, a real example is given and analysed as well. The area is situated in the transition zone of the Eastern Alps and the western Pannonian Basin, an interesting hilly region for tectonic geomorphological studies. The next section gives a short overview of the area providing also the tectonic geomorphic reasons why the area is suitable for the application of swath analysis.
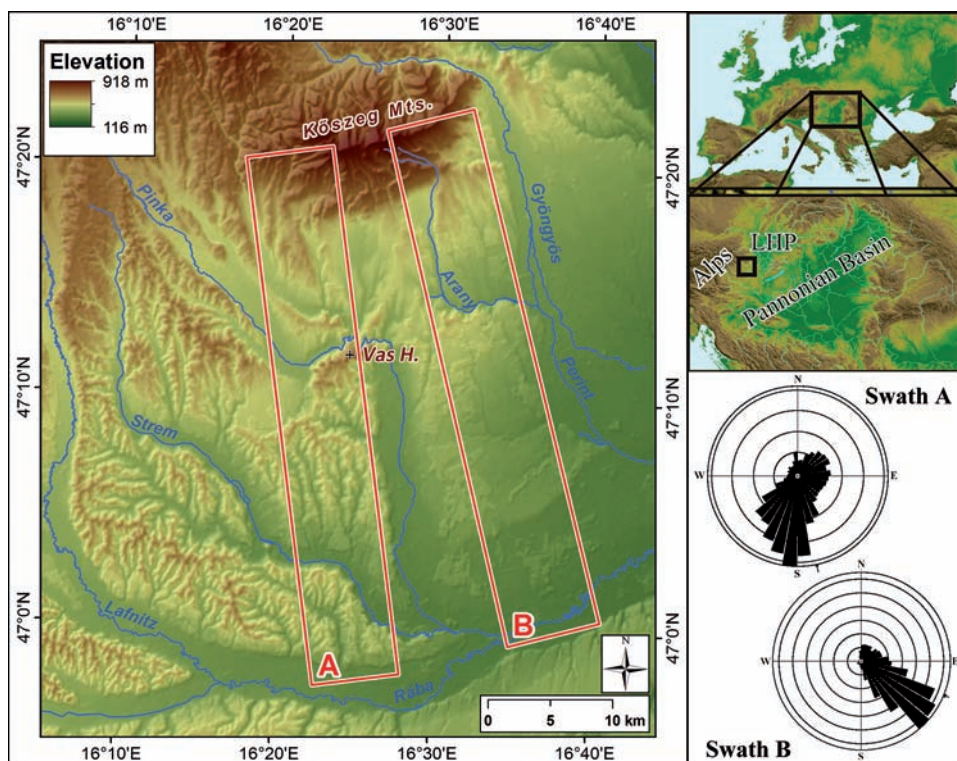


Fig. 7.   SRTM3 DTM of the studied Western Pannonian Alpine Foothills. Inset maps show the location of the study area (LHP: Little Hungarian Plain); red rectangles (A, B): selected swath boundaries. Rose diagrams are aspect frequencies of the studied swaths. Aspect directions were calculated from a 1,350 m radius mean-filtered topography to avoid biasing effect of small-scale landforms.

### 4.2.1    *Geological-geomorphic settings of the case study area*

The case study area (fig. 7) is situated in the western margin of the Pannonian Basin, in western Hungary and eastern Austria. It belongs to the Eastern Alpine Foreland, which is a hilly landscape with some lower mountains. Most part of the study area is covered by Miocene marine and lacustrine sediments (sand, clay, gravel). During the Pleistocene, alpine rivers reaching the foreland deposited here large amounts of gravelly sediments (e. g. PASCHER 1999). Two parts of the crystalline Penninic nappe, the Kőszeg Mts. (highest peak 882 m a.s.l.) and the Vas Hill crop out as tectonic windows from the younger sedimentary rocks. From tectonic geomorphic point of view it is important to emphasize that these areas are found to be slightly uplifting at present (Joó 1992), however, according to fission-track measurements (DUNKL & DEMÉNY 1997) their exhumation rate was highest during the Early Miocene.

Geomorphically, the hilly study area can be divided into two parts, which are later compared by swath analysis, too. The division line between these parts is the lower course of the river Pinka. East of this line, there is a low hilly landscape consisting of small plateau-like terrains. Both drainage density and relief are generally low within this part (mean relief is 20 m/km$^2$ – in this case, the relief is calculated as the elevation range within a 1 km$^2$ circle). The area is slightly tilted to the SSE, in general, but the dominant aspect is more to the S in the western part and more to the SE in the eastern part (see rose diagrams in fig. 7). The principal drainage direction (lower Pinka, river Perint and smaller valleys) is towards SSE, which means that the principal valley directions are not perfectly controlled by the dominant aspect. At many locations, secondary ENE-directed streams (e. g. the lower course of Arany, the central course of Pinka) cut the main NNW-SSE trend. These streams have asymmetric valleys with gently dipping northern sides and steeper southern slopes. According to JASKÓ (1948), ÁDÁM (1962) and our earlier work (KOVÁCS et al. 2008) these asymmetric valleys have been formed due to Quaternary faults, however, in his later work JASKÓ (1995) supposed cuesta-like formation as a result of differential erosion. West of the lower course of Pinka river, the terrain is more uplifted (by ~ 50 m) with much higher relief (mean relief is 53 m/km$^2$) and intense fluvial dissection. However, ridges are supposed to have preserved the Post-Pannonian paleo-surface. Drainage directions are mostly N-S and NW-SE. In many river valleys, southern and southwestern sides are steep, whereas northern and northeastern sides are less steep.

This case study area was selected because the analysis of tilted surfaces is a typical swath application. It is also advantageous that the more dissected western and the less dissected eastern parts offer a good opportunity to compare swath profile capabilities in tilted surface analysis. Basically, the existence, position, height and slope of steps and tilted surfaces are the main questions in this case and in many similar studies, so further analysis is focused on these problems.

### 4.2.2    *Swath profiles of the case study area*

Two swaths (*A* and *B*, fig. 7) were selected to represent the western and eastern parts of the study area. Swath orientations were set parallel to the main NNW-SSE valley orientation and orthogonal to the WSW-ENE crossing valleys. Although both swath rectangles originally include Kőszeg Mts., the northernmost 5 km are not represented
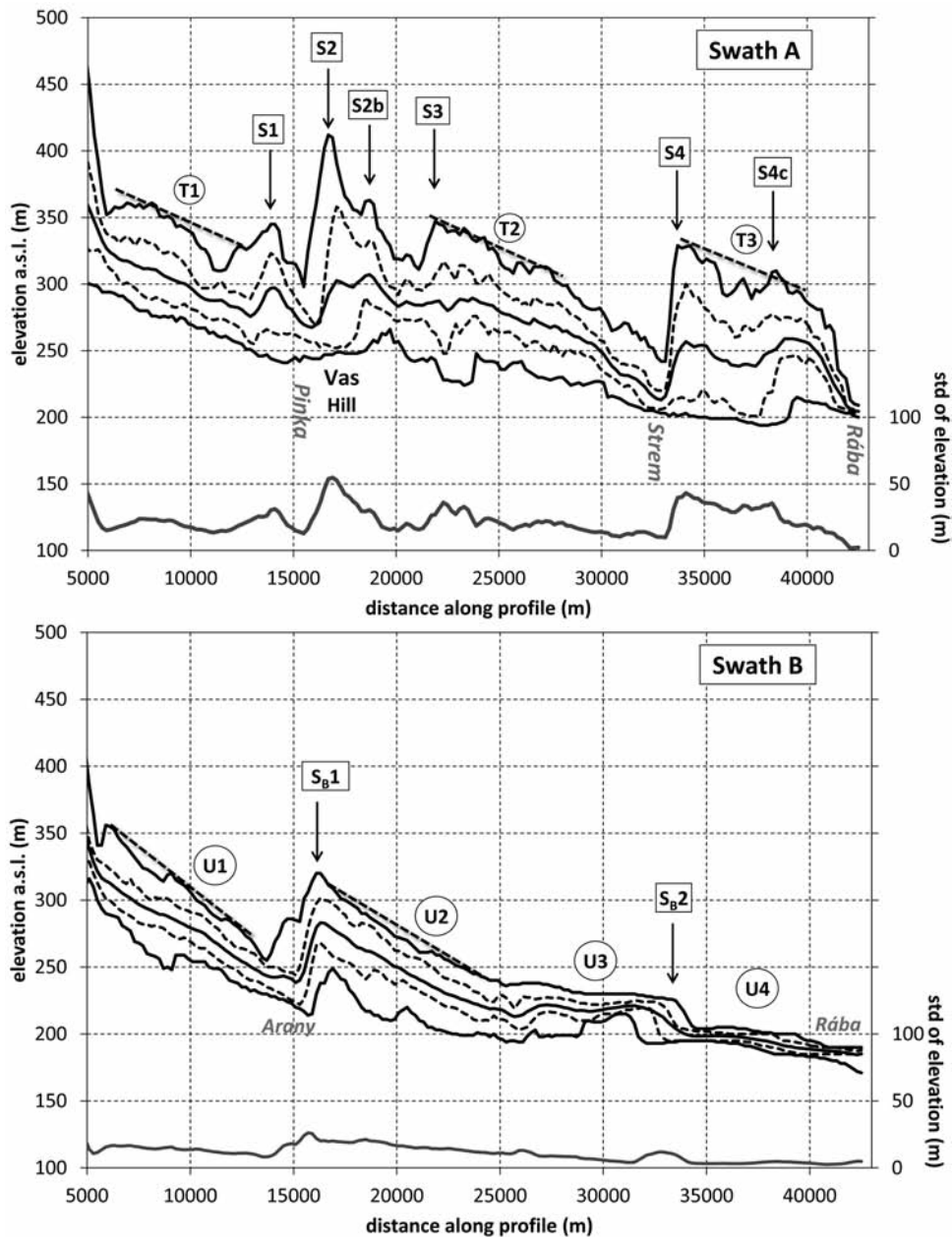
Fig. 8.   Swath profiles of the Western Pannonian Alpine Foothills. A: western swath profile; B: eastern swath profile. $T_i$ marks tilted surface; $S_i$ marks north-facing step (except $S_B2$ facing to south); $U_i$ marks terrain unit.

in the graphs (fig. 8 and further) in order to increase the vertical scale for the hilly terrain, which is studied in details. Original swath lengths were 42.5 km, whereas widths were 7 km and 7.5 km, respectively, so that the swaths contain laterally relatively homogeneous terrains. Strip width was set to 200 m. The resulting swath profiles are presented in fig. 8.

In the eastern swath *B* profile (fig. 8b) four terrain units can be delimited, the first two units (*U1* and *U2*) have an obvious tilt (0.70° and 0.52° respectively), whereas the two latter ones (*U3*, *U4*) are almost horizontal with a very slight tilt towards SSE. The first two units are divided by a sharp NNW-facing, 50 m high step ($S_B1$), which is expressed in all curves. The Quaternary tectonic origin of this step was proved by positional analysis of lignite layers (Kovács et al. 2008). At the southern end of *U2*, there is a break in all curves but without a vertical displacement that is typical for the boundary zones between tilted surfaces and depositional units. Finally, $S_B2$, a SSE-facing step marks the transition between *U3* and *U4*. It is a fluvial erosional edge. Its profile signal is shifted in the different curves that is due to the fact that this step is not perfectly orthogonal to the swath direction, the same phenomenon as in the artificial surface testing. As for the minimum curve, several further smaller steps are observed (at 9.3, 20.1, 26.3 and 28.9 km), these mark minor streams flowing out of the swath rectangle.

Due to the more dissected terrain, the remnant tilted surfaces are more difficult to recognize in the western sector based solely on the DEM. However, with the help of swath *A* profile (fig. 8a), it is much easier to identify these surfaces (*T1*, *T2* and *T3* with tilt angles of 0.54°, 0.38° and 0.33°, respectively). In this case, even the maximum curve is touched by erosion, but long linear sections (especially in the mean curve) define clearly enough the southward sloping surfaces. *T3* is somewhat special, because the eastern third of this segment belongs to the low-elevation Strem valley. Due to this biasing effect, the lower quartile (Q1) and minimum values are significantly decreased. The Vas Hill unit (where the Penninic metamorphic rocks outcrop) implies the largest relief (STD) in swath *A* and its summit level is obviously above the *T2* trend. On the contrary, the Strem valley is depressed below this trend. North-facing steps are also detected (*S1–S4c*), the most important being *S2* and *S4* with height difference of 114 m and 87 m, respectively, in the maximum curve. These steps are characterized by the highest STDs, too. Due to the oblique crossing of Pinka at *S2* the increase of the Q1 and minimum curves are shifted southwards. At *S4*, the turn of Strem to the South results in a continuously decreasing minimum trend, a situation very similar to the artificial test *C* swath. Small horizontal segments in the upper quartile (Q3) and mean curve at 32 km are linked to Strem river terraces. In the sensitivity analysis, the reference swath is the 7 km wide swath *A*.

### 4.2.3 *Sensitivity to swath width*

The location of the different width swaths can be seen in fig. 9. The 1 km wide swath is limited to a narrow path only, whereas the largest rectangle contains terrains quite different from the central part (e. g. lower Pinka valley).

As for the comparison of mean profiles (fig. 10), the two narrowest (1 and 4 km) swaths result in more oscillating curves, especially the 1 km-wide swath produces higher peaks, and less frequently, deeper valleys. For the other four curves, differ-
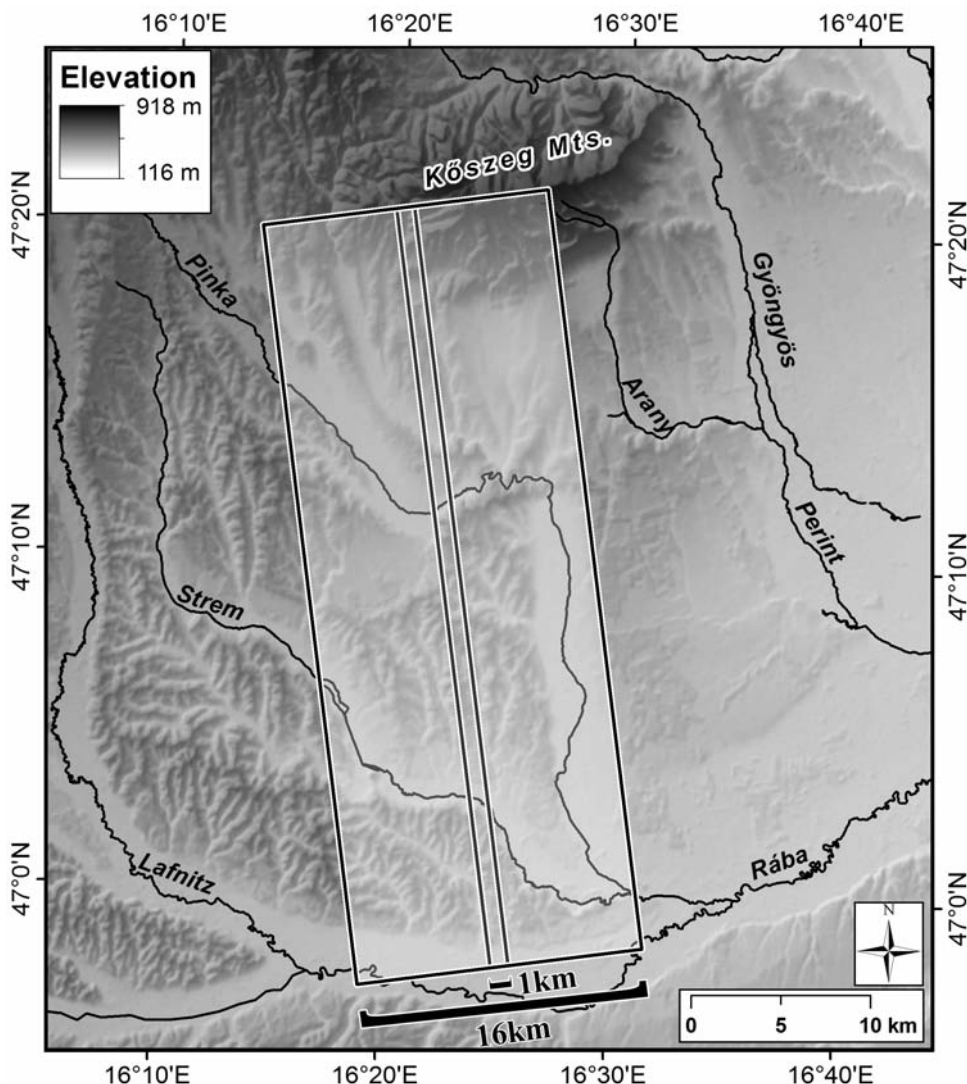
Fig. 9.   Widest and narrowest swath rectangles of swath width sensitivity analysis.

ences are much smaller, although *T2* surface is seemingly lower as the wider swaths capture the lower Pinka valley. The normalized RMSE values (table 1) support the previous statement, since general deviations are below 7.4%, except in case of the narrowest swath, where it is 12.9%. The SEM values are mostly less than 2 m that justifies that mean values characterize the surface with satisfying reliability. Here again, the narrowest swaths produce significantly higher SEMs. It is also observed that SEM peaks usually coincide with abrupt topographic changes; nevertheless it is not surprising, since STD is also high at topographic changes, whereas the sample size, i. e. swath width is constant for a given rectangle.

Fig. 10.    Comparison diagrams of swath width sensitivity analysis. W means width.

Table 1.     RMSE values of the mean, max and STD curves between the reference (swath *A*, 7 km wide, 172° azimuth) and the corresponding profile.

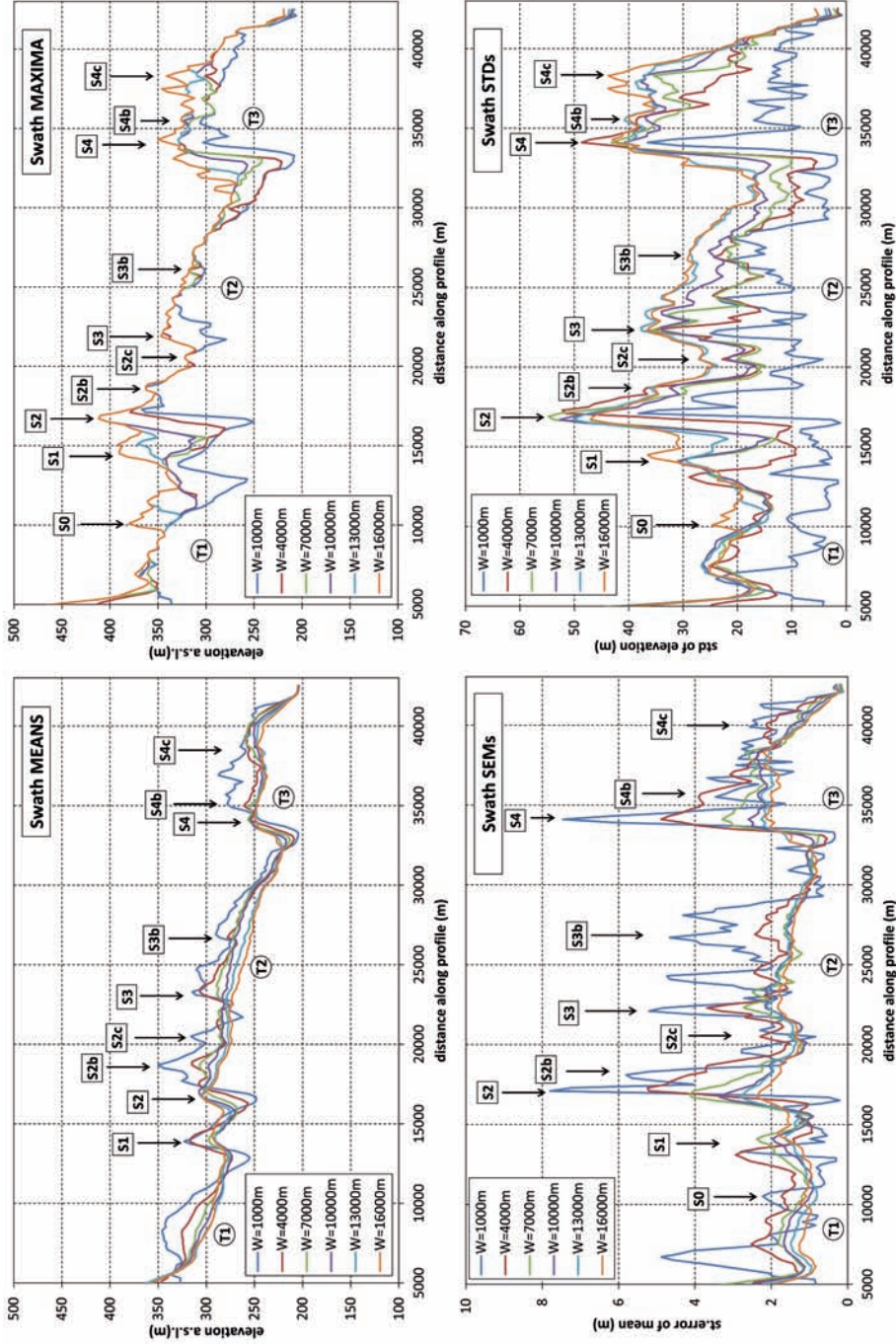| Statistic | Curve Type | Varying width versions | | | | | Differing azimuth versions | | | |
|---|---|---|---|---|---|---|---|---|---|---|
| | | 1 km | 4 km | 10 km | 13 km | 16 km | 162° | 167° | 177° | 182° |
| RMSE | Mean | 19.5 | 7.3 | 4.7 | 8.6 | 11.1 | 11.4 | 6.4 | 6.5 | 11.8 |
| norm.RMSE | Mean | 12.9% | 4.9% | 3.1% | 5.6% | 7.4% | 7.4% | 4.2% | 4.2% | 7.9% |
| RMSE | Max | 32.2 | 15.2 | 8.5 | 18.5 | 24.2 | 14.5 | 8.8 | 10.4 | 14.2 |
| norm.RMSE | Max | 13.5% | 6.4% | 3.6% | 7.8% | 10.3% | 6.1% | 3.7% | 4.4% | 6.0% |
| RMSE | Std | 14.3 | 6.0 | 3.3 | 6.4 | 7.6 | 6.1 | 3.8 | 3.7 | 6.4 |
| norm.RMSE | Std | 26.6% | 11.2% | 6.3% | 12.0% | 14.3% | 11.6% | 7.2% | 6.5% | 11.9% |

The maximum curves (fig. 10) show larger differences. As new terrains are added horizontally to the swath, the corresponding maximum levels are reached at shorter profile distances. As a result, the position and height of topographic peaks are altered. In this case again the narrowest swath results the most deviating profile. The normalized RMSE values are all higher: between 3.6% and 10.3%, except for the 1 km wide swath, where it is as high as 13.5%.

STD (fig. 10) is an even more sensible statistic, differences are still larger. Although the tendencies are rather similar in each curve, the amplitudes are different. Naturally, STD is significantly smaller for the narrowest swath. The two widest swaths produce similar and relatively high STDs because these include some parts of the low-elevation lower Pinka valley. Normalized RMSE values are between 6.3% and 14.3% (except the highest value, 26.6% linked to the narrowest swath, again) supporting the sensibility of this statistic.

Calculated surface tilts are very low (~ 0.5°) in all cases (table 2). In general, values do not deviate more than 0.1° from the reference value; however, as the reference value is very low, these deviations are relatively high. There are segments, where the maximum curves of the different width swaths coincide; therefore the resulted tilt values are similar or equal. In most cases, values calculated from the mean curves are slightly smaller. Obviously, the narrowest swath performs less powerful.

North-facing steps (table 3) are detected more or less at similar profile distances by each curve. On the other hand, step heights are more diverse. In 54% of all cases, the difference from step height value based on the reference curve is less than 10 m, but for 20% the difference is greater than 20 m. In general, heights calculated based on the mean curves are significantly smaller (~ 50–70%) than values based on the maximum curves. The important steps (*S1*, *S2*, *S3*, *S4*) are recognizable in almost all curves, but certain features are present in the widest or in the narrowest swaths, only. Typically, several minor "extra" peaks are related to the 1 km wide swath profile. These arbitrary landforms merge into larger units when swath width is enlarged.

### 4.2.4 *Sensitivity to swath orientation*

The location of the different angle swaths can be seen in fig. 11, the comparison dia-
grams are presented in fig. 12. It is observed that swath profile curves are rather
similar to each other in the central segments. Larger deviations among the curves are
observed only in the southern parts, where the ratio of the higher hilly terrain and the
low-elevation Strem valley is quite different in each swath. This varying ratio causes
differences mainly in the mean curves, however, the maximum curves are also signif-
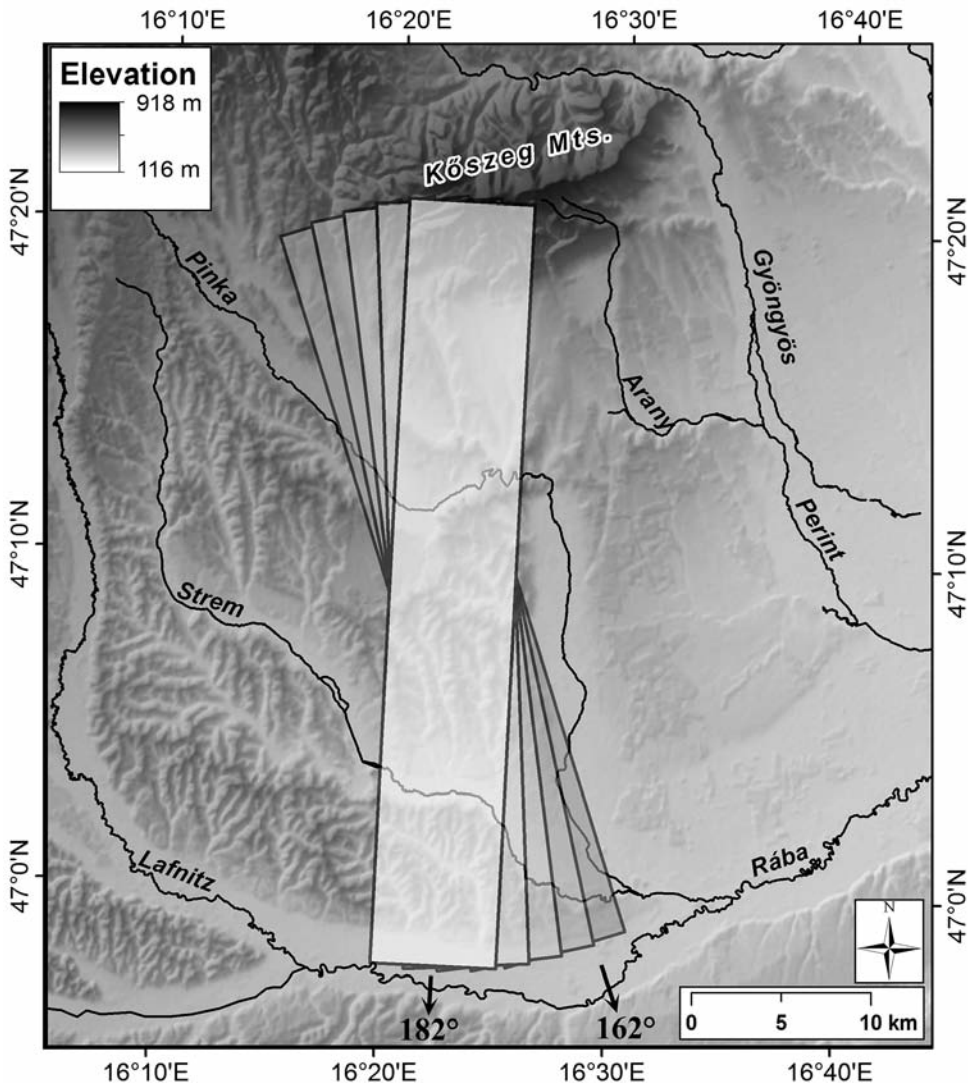icantly changed at around 33 km, since in case of the more easterly swaths (A = 162°,



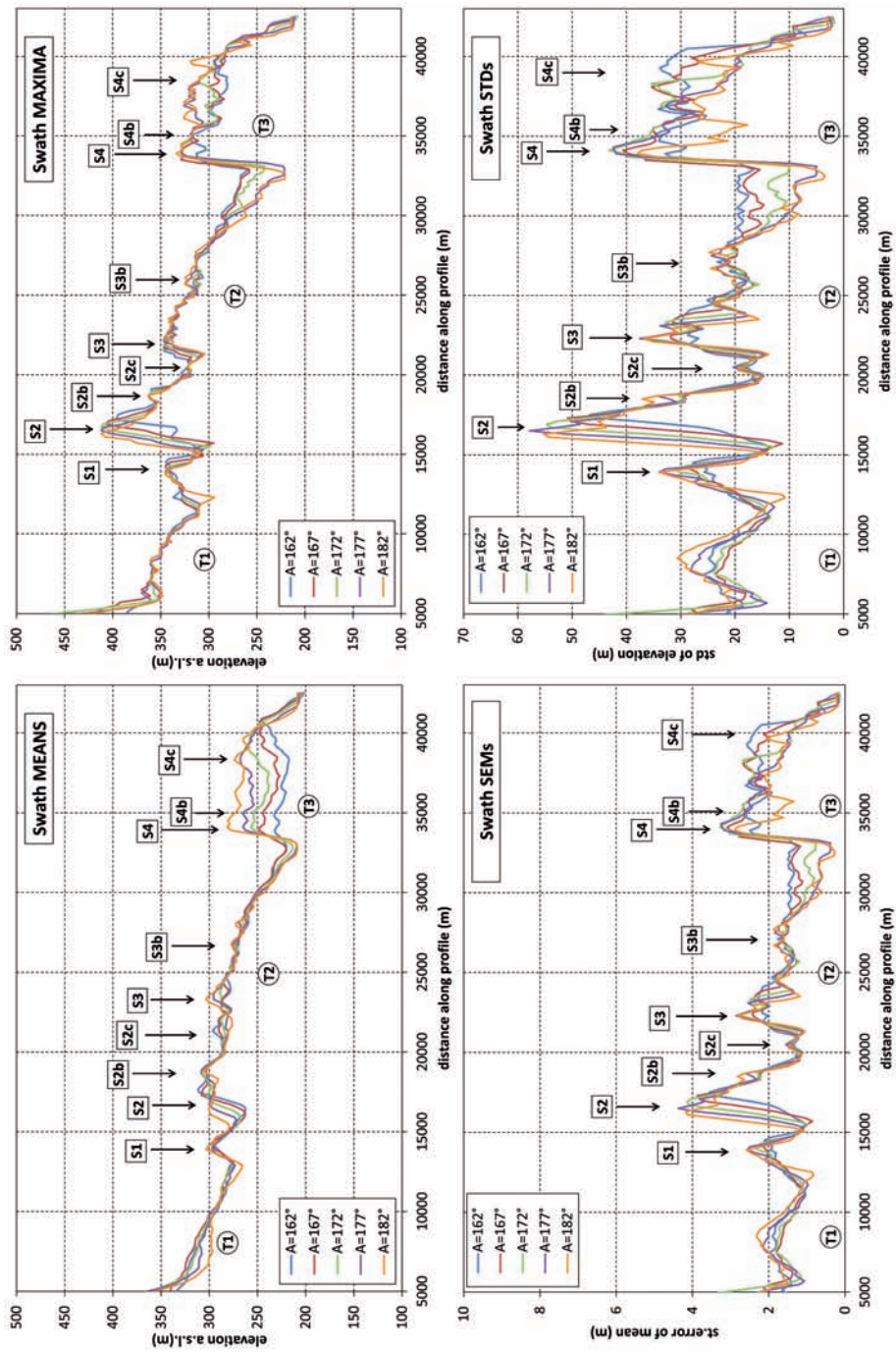Fig. 11.   Swath rectangles of swath orientation sensitivity analysis.

Fig. 12. Comparison diagrams of swath orientation sensitivity analysis. 'A' means azimuth.

Table 2.    Tilt values (°) for the tilted surfaces calculated from the swath profiles. Tilt is cal-
            culated from the elevations at profile distances given in the table. The reference is
            swath *A* (7 km wide, 172° azimuth).

| Tilt Id | Curve Type | Profile distance | Reference | Varying width versions | | | | |
|---------|------------|------------------|-----------|------|------|-------|-------|-------|
|         |            |                  |           | 1 km | 4 km | 10 km | 13 km | 16 km |
| T1(°) | Mean | 6,900–9,700 | 0.35 | 0.16 | 0.25 | 0.43 | 0.43 | 0.42 |
| T2(°) | Mean | 23,700–29,500 | 0.33 | 0.38 | 0.50 | 0.26 | 0.29 | 0.25 |
| T3(°) | Mean | 34,100–36,900 | 0.35 | −0.87 | 0.16 | 0.25 | 0.22 | 0.25 |
| T1(°) | Max | 7,900–9,500 | 0.54 | 0.54 | 0.54 | 0.54 | 0.54 | 0.54 |
| T2(°) | Max | 24,100–27,300 | 0.38 | 0.38 | 0.38 | 0.38 | 0.38 | 0.38 |
| T3(°) | Max | 33,900–39,500 | 0.33 | 0.19 | 0.30 | 0.33 | 0.33 | 0.33 |

| Tilt Id | Based on | Profile distance | Reference | Differing azimuth versions | | | |
|---------|----------|------------------|-----------|------|------|------|------|
|         |          |                  |           | 162° | 167° | 177° | 182° |
| T1(°) | Mean | 6,900–9,700 | 0.35 | 0.47 | 0.45 | 0.21 | 0.08 |
| T2(°) | Mean | 24,700–29,500 | 0.34 | 0.35 | 0.32 | 0.31 | 0.34 |
| T3(°) | Mean | 34,100–36,900 | 0.35 | 0.13 | 0.36 | 0.14 | 0.32 |
| T1(°) | Max | 7,900–9,900 | 0.54 | 0.43 | 0.49 | 0.52 | 0.46 |
| T2(°) | Max | 22,300–27,300 | 0.36 | 0.30 | 0.36 | 0.36 | 0.39 |
| T3(°) | Max | 33,700–40,100 | 0.39 | 0.26 | 0.39 | 0.30 | 0.37 |

167° and partly 172°), the maximum elevations are linked to a small interfluvial ridge
between Pinka and Strem valleys (best observable in fig. 7), therefore, the valley bot-
tom remains hidden in these curves. A further consequence of these differences is that
SEM and STD curves are also dissimilar in this segment.

     Numerically, the normalized RMSE values show that 5° change causes ~ 4 %
deviation in both the mean and maximum curves and ~ 7 % deviation in the STD
curves. 10° change causes ~ 7.5 % change in the mean profiles, ~ 6 % change in the
maximum and ~ 12 % change in the STD profiles. It is noted that RMSE deviations
are symmetrical for the reference swath, an observation, which is not true for width
sensitivity.

     Calculated tilt values are in the same range as in the previous analysis with devi-
ations from the reference values usually less than 0.1°. Here again, maximum-based
tilt values are closer to each other. In principle, if swath azimuth coincides with the
direction of maximum tilt, deviations from the reference values should be negative.
Since it is true for most values, it is stated that the reference swath azimuth was well
chosen to study the tilted surface topography.

     Major steps (*S1*, *S2*, *S3*, *S4*) are recognizable in almost all curves. Step positions
and heights are somewhat more homogeneous than in the width sensitivity analysis.
In 63 % of all cases, the difference from reference step height value is less than 10 m,
whereas the difference is greater than 20 m for 13 % of the cases, only. However, at
*S4*, due to the mixing of different terrains, as mentioned above, step parameters are
more varied than in the width sensitivity analysis. Furthermore, at *S3*, the alteration

Table 3.  North-facing step positions (profile distance) and heights (*dh*). Threshold heights are 15 m for the mean curves and 25 m for the maximum curves. Certain steps are divided into two smaller parts, in these cases, heights are added but two profile distances are marked in the table.

| Step Id | Width versions, MEAN | | | Width versions, MAX | | | Azimuth versions, MEAN | | | Azimuth versions, MAX | | |
|---|---|---|---|---|---|---|---|---|---|---|---|---|
| | Curve Id | Prof.Dist. | dh | Curve Id | Prof.Dist. | dh | Curve Id | Prof.Dist. | dh | Curve Id | Prof.Dist. | dh |
| S0 | | | | 13 km | 11500 | 34 | | | | | | |
| S0 | | | | 16 km | 10100 | 37 | | | | | | |
| S1 | 1 km | 13900 | 68 | 1 km | 13900 | 72 | 162° | 14300 | 20 | | | |
| S1 | 4 km | 13900 | 43 | 4 km | 14100 | 32 | 167° | 14300 | 22 | | | |
| S1 | 7 km | 14100 | 21 | 10 km | 13900 | 35 | 172° | 14100 | 21 | | | |
| S1 | 10 km | 14100 | 18 | 13 km | 15100 | 42 | 177° | 13900 | 24 | 177° | 13700 | 35 |
| S1 | | | | 16 km | 15100 | 62 | 182° | 13900 | 38 | 182° | 13700 | 51 |
| S2 | 1 km | 17700 | 77 | 1 km | 17300 | 117 | 162° | 17700 | 49 | 162° | 16100; 17300 | 95 |
| S2 | 4 km | 17500 | 51 | 4 km | 17100 | 99 | 167° | 17300 | 46 | 167° | 16900 | 112 |
| S2 | 7 km | 17100 | 35 | 7 km | 16700 | 114 | 172° | 17100 | 35 | 172° | 16700 | 114 |
| S2 | 10 km | 17100 | 38 | 10 km | 16700 | 101 | 177° | 16700 | 28 | 177° | 16500 | 106 |
| S2 | 13 km | 16700 | 32 | 13 km | 16700 | 61 | 182° | 16500 | 21 | 182° | 16300 | 105 |
| S2 | 16 km | 16700 | 23 | 16 km | 16700 | 45 | | | | | | |

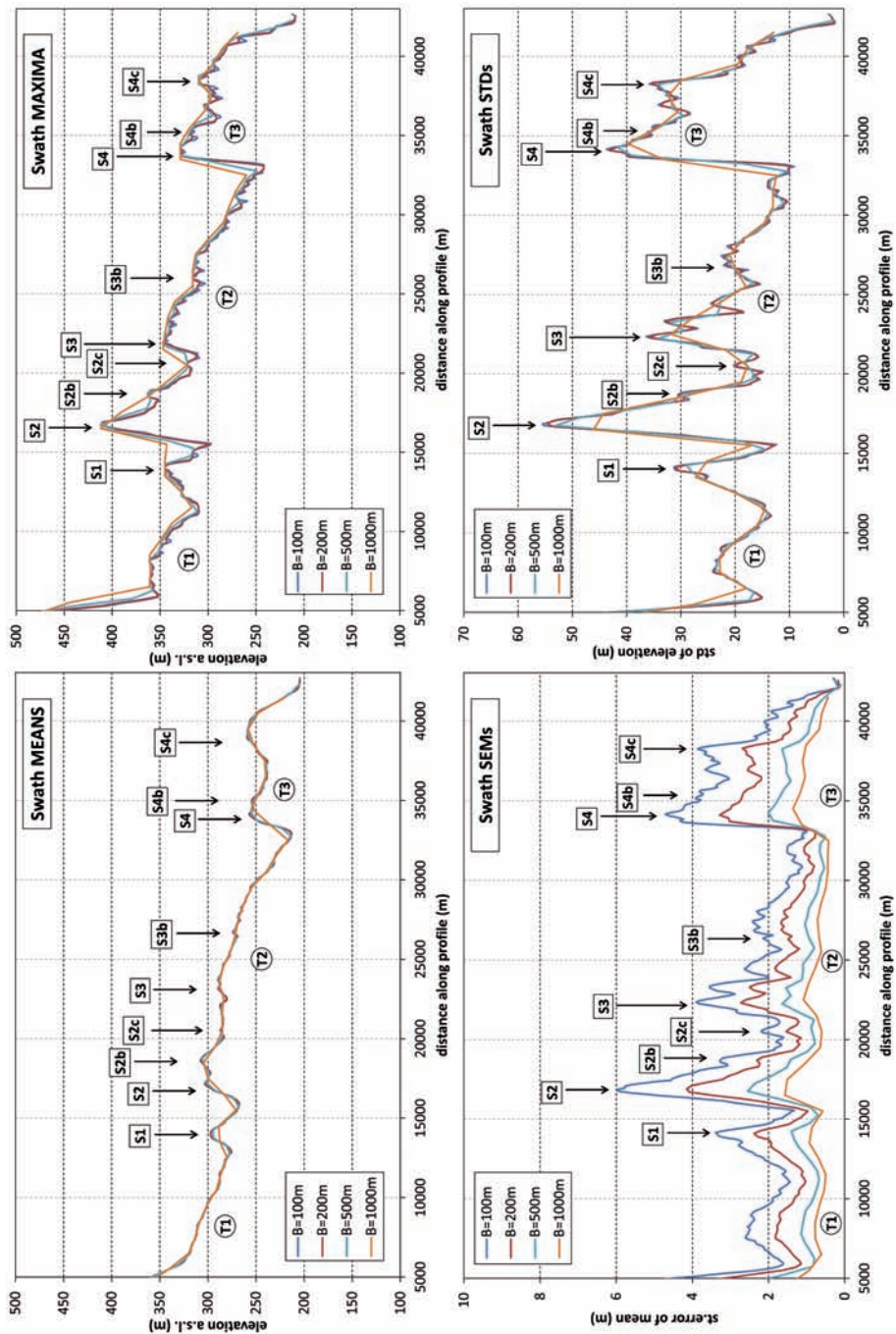| Profile | Dist | Val | n | Dist | Val | n | Az | Val | n | Az | Val | n |
|---|---|---|---|---|---|---|---|---|---|---|---|---|
| S2b | 1 km | 18700 | 25 | | | | | | | | | |
| S2b | 4 km | 18700 | 15 | | | | | | | | | |
| S2c | 1 km | 20500 | 15 | | | | | | | | | |
| S3 | 1 km | 23300 | 52 | 4 km | 22100 | 34 | 177° | 23500 | 15 | 162° | 21500 | 29 |
| S3 | 4 km | 23300 | 31 | 7 km | 21900 | 36 | 182° | 23300 | 27 | 167° | 21700 | 29 |
| S3 | | | | 10 km | 21900 | 36 | | | | 172° | 21900 | 36 |
| S3 | | | | 13 km | 21900 | 36 | | | | 177° | 22100 | 41 |
| S3 | | | | 16 km | 21900 | 36 | | | | 182° | 22300 | 43 |
| S3b | 1 km | 26900 | 16 | 1 km | 24300 | 40 | | | | | | |
| S4 | 1 km | 35700 | 75 | 1 km | 34100 | 95 | 167° | 33900 | 29 | 162° | 33900 | 55 |
| S4 | 4 km | 34100 | 47 | 4 km | 34300 | 108 | 172° | 34100 | 44 | 167° | 33500 | 71 |
| S4 | 7 km | 34100 | 44 | 7 km | 33700 | 87 | 177° | 34100 | 56 | 172° | 33700 | 87 |
| S4 | 10 km | 34100 | 37 | 10 km | 33700 | 72 | 182° | 34100 | 73 | 177° | 33900 | 108 |
| S4 | 13 km | 34100 | 29 | 13 km | 33100 | 69 | | | | 182° | 33900 | 113 |
| S4 | 16 km | 34300 | 29 | 16 km | 33100; 34300 | 97 | | | | | | |
| S4b | 1 km | 36900 | 25 | 1 km | 35300 | 29 | | | | | | |
| S4b | | | | 16 km | 37500 | 34 | | | | | | |
| S4c | 4 km | 39300 | 16 | | | | 162° | 40700 | 29 | | | |
| S4c | 7 km | 39100 | 21 | | | | 167° | 40700 | 18 | | | |
| S4c | | | | | | | 172° | 39100 | 21 | | | |

Fig. 13.    Comparison diagrams of swath bin size sensitivity analysis. 'B' means bin size (strip width).

of width does not change the maximum curve; therefore at this point the step parameters based on the different width maximum curves are inimitably homogeneous.

### 4.2.5 *Sensitivity to swath horizontal resolution (i. e. bin size or strip width)*

Fig. 13 presents swath *A* profile curves calculated using different bin sizes In general, peaks and valleys are smoothed and slopes are reduced as bin size increases. It is clearly observable in the mean curves (fig. 13), but this smoothing effect is significant only at the largest, 1,000 m, bin size in the given example. As for the maximum curves, a kind of envelope surface is approached with increasing bin size. STD curves indicate that STD does not significantly change at intermediate elevations, but high and low values are smoothed as in case of the mean curves. Again, this effect is the most remarkable at the 1,000 m bin size. Finally, the constant STD and the increasing number of points in each bin result that SEMs are decreased as bin size increases. This decrease is characteristic even at minor changes of bin size (from 100 to 200 m). It implies that precision of the mean curve can be effectively improved by growing the bin size, but this, in turn, reduces the topographic details.

## 5 *Discussion*

There is a growing number of studies using swath profile analysis, but none of them discusses the statistical reliability of this method. Most authors determine swath rectangles intuitively. Based on the above result, we suggest that at similar scaled DEMs a minimum swath width (4 km in the given example) is required to avoid arbitrary peaks and to capture larger pieces of remnant surfaces. It is similar to the opinion of Musumeci et al. (2003) who remarked that swath width should be large enough to avoid problems related to the influence of different river orientations; therefore more than just one valley should be included in the swath. Based on a somewhat different principle, Kühni & Pfiffner (2001) argued that local relief converges to a constant value as width increases to 10–30 km (Central Alps), therefore choosing a wide enough swath ($> 30$ km) ensures that the resulting local relief will be the maximum value for the area examined. However, if the tectonic units are elongated on the surface (cf. Lucazeau & Hurtrez 1997), this may influence the appropriate swath width selection.

On the other hand, the maximum width is determined by the extension of the studied terrain units. Based on graphical and statistical analysis of the studied example (the Western Pannonian Alpine Foothills), we found that swath profiles and calculated step and tilt values were within an acceptable range for width between 4 and 13 km and especially, the 10 and 13 km wide swaths resulted highly similar values and graphs. The maximum curves and the values (e. g. step heights) derived from these are highly robust, if a minimum width is reached at which the swath contains the most outstanding ridges. This example shows that swath profile analysis is only slightly sensitive to swath width within a reasonable range, which is linked to landscape scale.

Both artificial and real examples proved that linear features orthogonal to swath direction are best recognized in the swath profile. This must be taken into consideration when swath profiles are analyzed. As for the orientation sensitivity, we found

that even 10° change in swath azimuth produces acceptable differences in the profiles (< 8 % rel. RMSE in the means; < 6 % rel. RMSE in the maxima) and in the derived values.

When choosing swath bin size one has to find the compromise between the need for details and precise characterization of larger surfaces. In fact, the maximum curve, which is often used as the discriminator of remnant surfaces, is only slightly influenced by swath bin size, and approaches an envelope surface as bin size is increased.

These results related to sensitivity support a flexible use of swath analysis. However, for a sophisticated study, the method applied in this paper can be recommended to find the optimal width and azimuth. The analysis can be carried out at several width and azimuth and the one in which the curves deviate least from others can be chosen as optimal for width and the one in which the tilt values are the highest and/or the orthogonal linear features are the most remarkable can be chosen as optimal for azimuth. If the azimuth of the analysed features is not constant in the region, a curvilinear swath analysis may solve the problem.

The artificial surface test demonstrated that a remnant surface can be sufficiently reconstructed based on the maximum curve even if it is disturbed or interrupted by erosional landforms. On the contrary, vertical faulting changed the trend of all curves in the swath profile. Similar phenomena can be detected in real surfaces as well (e. g. north-facing steps in the Western Pannonian Alpine Foothills). However, a parallel step in all curves may be attributed to other landforms, too (e. g. cuestas).

## 6     *Conclusions*

There is a trend in today's GIS/geomorphometry to pile up large bulk of data and to apply more complicated derivatives and parameters. These new methods certainly help to understand new aspects of geomorphology, nonetheless, in the increasing complexity there is a need for data reduction, a tool of simplification. Topographic swath profile analysis admittedly points into this direction. Basically, it reduces (quasi-)3D phenomena into 2D. It is a simple tool that helps to recognize and quantify general surface trends, incisions and other topographic effects. The main strength of this method is most likely its conciseness. Correlations between several parameters (topography, precipitation, exhumation, uplift, etc.) are also easy to observe in swath profiles, either visually or statistically.

However, in most cases, it does not stand alone and it must be completed by additional methods, such as hypsometric analysis (Strahler 1952), slope vs. elevation analysis (e. g. Korup et al. 2005), grid correlations and envelope surface analysis (e. g. Burbank & Anderson 2001, Székely 2003). Nevertheless, none of the previously mentioned methods show directional variations, that is a further advantage of swath profile analysis.

To encourage the use of this method in future studies, we presented here a detailed assessment of the methodology that we consider to be a step towards a standardized way of application. It is also demonstrated how this analysis can be extended to curvilinear or circular landforms, such as large orogens or volcanoes. Sensitivity analysis in this paper proved that the swath analysis tolerates relatively large changes in width (~ 5 km in the study example) and azimuth (~ 10° in the study example), that supports the robustness of this method.

# References

ÁDÁM, L. (1962): A Rábántúli kavicstakaró. – In: Ádám, L., Góczán, L., Marosi, S., Somogyi, S., Szilárd, J.: Néhány dunántúli geomorfológiai körzet jellemzése. – Földrajzi Értesítő **11**(1): 41–52 (in Hungarian).

BISHOP, M. P., SHRODER, J. F. & COLBY, J. D. (2003): Remote sensing and geomorphometry for studying relief production in high mountains. – Geomorphology **55:** 345–361.

BOOKHAGEN, B., THIEDE, R. C. & STRECKER, M. R. (2005): Abnormal monsoon years and their control on erosion and sediment flux in the high, arid northwest Himalaya. – Earth and Planet. Sci. Lett. **231:** 131–146.

BURBANK, D. W. & ANDERSON, R. S. (2001): Tectonic Geomorphology. – Blackwell Science, 274 pp.

CHAMPAGNAC, J.-D., SCHLUNEGGER, F., NORTON, K., VON BLANCKENBURG, F., ABBÜHL, L. M. & SCHWAB, M. (2009): Erosion-driven uplift of the modern Central Alps. – Tectonophysics **474:** 236–249.

DORTCH, J. M., OWEN, L. A., SCHOENBOHM, L. M. & CAFFEE, M. W. (2011): Asymmetrical erosion and morphological development of the central Ladakh Range, northern India. – Geomorphology **135:** 167–180.

DUNKL, I. & DEMÉNY, A. (1997): Exhumation of the Rechnitz Window at the border of the Eastern Alps and Pannonian Basin during Neogene extension. – Tectonophysics **272:** 197–211.

FIELDING, E., ISACKS, B., MUAWIA, B. & DUNCAN, C. (1994): How flat is Tibet? – Geology **22:** 163–167.

FIELDING, E. J. (1996): Tibet uplift and erosion. – Tectonophysics **260:** 55–84.

FOSTER, D., BROCKLEHURST, S. H. & GAWTHORPE, R. L. (2008): Small valley glaciers and the effectiveness of the glacial buzzsaw in the northern Basin and Range, USA. – Geomorphology **102:** 624–639.

GODARD, V., LAVÉ, J., CARCAILLET, J., CATTIN, R., BOURLES, D. & ZHU, J. (2009): Spatial distribution of denudation in Eastern Tibet and regressive erosion of plateau margins. – Tectonophysics **491**(1–4): 253–274.

GROHMANN, C. H. (2004): Morphometric analysis in geographic information systems: applications of free software GRASS and R. – Computers and Geosciences **30:** 1066–1067.

GROHMANN, C. H., RICCOMINI, C. & CHAMANI, M. A. C. (2011): Regional scale analysis of landform configuration with base-level (isobase) maps. – Hydrol. and Earth System Sci. **15:** 1493–1504.

HOKE, G., ISACKS, B. L. & JORDAN, T. E. (2005): Equilibrium landscapes of the western Andean mountain front (10° S–33° S): Long-term responses to along-strike changes in dimate. – 6th International Symposium on Andean Geodynamics (ISAG 2005, Barcelona), Extended Abstracts, 386–389.

HOKE, G. D. & GARZIONE, C. N. (2008): Paleosurfaces, paleoelevation, and the mechanisms for the late Miocene topographic development of the Altiplano plateau. – Earth and Planet. Sci. Lett. **271:** 192–201.

Houser, C. & Mathew, S. (2011): Alongshore variation in foredune height in response to transport potential and sediment supply: South Padre Island, Texas. – Geomorphology **125:** 62–72.

Jaskó, S. (1948): A nyugatvasmegyei barnakőszén-terület. – Földrajzi Közlemények **78:** 112–120 (in Hungarian with German abstract).

Jaskó, S. (1995): A Kárpátmedence nyugati szegélyének neotektonikája. – Földtani Közlöny **125**(3–4): 215–239 (in Hungarian with English abstract).

Johnson, C. B., Furlong, K. P. & Kirby, E. (2009): Integrated geomorphic and geodynamic modeling of a potential blind thrust in the San Francisco Bay area, California. – Tectonophysics **471:** 319–328.

Joó, I. (1992): Recent Vertical Surface Movements In The Carpathian Basin. – Tectonophysics **202:** 129–134.

Karátson, D., Telbisz, T. & Wörner, G. (2012): Erosion rates and erosion patterns of Neogene to Quaternary stratovolcanoes in the Western Cordillera of the Central Andes: An SRTM DEM based analysis. – Geomorphology **139–140:** 122–135.

Kienzle, S. (2004): The Effect of DEM Raster Resolution on First Order, Second Order and Compound Terrain Derivatives. – Transactions in GIS **8**(1): 83–111.

Korup, O., Schmidt, J. & McSaveney, M. J. (2005): Regional relief characteristics and denudation pattern of the western Southern Alps, New Zealand. – Geomorphology **71:** 402–423.

Kovács, G., Székely, B. & Papp, S. (2008): Observations of the surface evolution of Pinka Plain: mass movements and neotectonics. – In: Kaiser, H. K., Kirner, R. (Ed.) Proceedings of the Junior Scienist Conference 2008. Vienna, 309–310.

Kühni, A. & Pfiffner, O. A. (2001): The relief of the Swiss Alps and adjacent areas and its relation to lithology and structure: topographic analysis from a 250-m DEM. – Geomorphology **41:** 285–307.

Lin, Z. & Oguchi, T. (2006): DEM analysis on longitudinal and transverse profiles of steep mountainous watersheds. – Geomorphology **78:** 77–89.

Lucazeau, F. & Hurtrez, J. E. (1997): Length-scale dependence of relief along the southeastern border of Massif Central (France). – Geophys. Res. Lett. **24**(14): 1823–1826.

Munroe, J. S. (2006): Investigating the spatial distribution of summit flats in the Uinta Mountains of northeastern Utah, USA. – Geomorphology **75:** 437–449.

Musumeci, G., Ribolini, A. & Spagnolo, M. (2003): The effects of late Alpine tectonics in the morphology of the Argentera Massif (Western Alps, Italy–France). – Quatern. Internat. **101–102:** 191–201.

Pascher, G. A. (1999): Geologische Karte des Burgenlandes 1:200000. Geologische Bundesanstalt, Wien.

Pratt-Sitaula, B., Burbank, D. W., Heimsath, A. & Ojha, T. (2004): Landscape disequilibrium on 1,000–10,000 year scales Marsyandi River, Nepal, central Himalaya. – Geomorphology **58:** 223–241.

Rabus, B., Eineder, M., Roth, A. & Bamler, R. (2003): The shuttle radar topography mission – a new class of digital elevation models acquired by spaceborne radar. – Photogrammetric Remote Sensing **57:** 241–262.

Rehak, K., Strecker, M. R. & Echtler, H. P. (2008): Morphotectonic segmentation of an active forearc, 37°–41° S, Chile. – Geomorphology **94:** 98–116.

Robl, J., Hergarten, S. & Stüwe, K. (2008): Morphological analysis of the drainage system in the Eastern Alps. – Tectonophysics **460:** 263–277.

Staley, D. M., Wasklewicz, T. A. & Blaszczynski J. S. (2006): Surficial patterns of debris flow deposition on alluvial fans in Death Valley, CA using airborne laser swath mapping data. – Geomorphology **74:** 152–163.

Stolar, D. B., Willett, S. D. & Montgomery, D. R. (2007): Characterization of topographic steady state in Taiwan. – Earth and Planet. Sci. Lett. **261:** 421–431.

Strahler, A. N. (1952): Hypsometric (area–altitude) analysis of erosional topography. – Geol. Soc. of America Bull. **63:** 1117–1142.

Stüwe, K., Robl, J. & Matthai, S. (2009): Erosional decay of the Yucca Mountain crest, Nevada. – Geomorphology **108:** 200–208.

Székely, B. (2003): The Eastern Alps in an envelope – An estimation on the "missing volume". – N. Jb. Geol. Pal. Abh. **230**(2–3): 257–275.

Telbisz, T. (2011): Large-scale relief of the Slovak Karst and Aggtelek Karst (Gömör-Torna/ Gemer-Turňa Karst) – a DEM-based study. – Hungarian Geogr. Bull. **60**(4): 379–396.

Thiede, R. C., Bookhagen, B., Arrowsmith, J. R., Sobel, E. R. & Strecker, M. R. (2004): Climatic control on rapid exhumation along the Southern Himalayan Front. – Earth and Planet. Sci. Lett. **222:** 791–806.

Van der Beek, P. & Bourbon, P. (2008): A quantification of the glacial imprint on relief development in the French western Alps data. – Geomorphology **97:** 52–72.

Wegmann, K. W. & Pazzaglia, F. J. (2009): Late Quaternary fluvial terraces of the Romagna and Marche Apennines, Italy: Climatic, lithologic, and tectonic controls on terrace genesis in an active orogen. – Quatern. Sci. Rev. **28:** 137–165.

Zhang, W., Drake, N., Wainwright, J. & Mulligan, M. (1999): Comparison of slope estimates from low resolution DEMs: Scaling issues and a fractal method for their solution. – Earth Surf. Proc. and Landf. **24:** 763–779.

Addresses of the authors: T. Telbisz, Department of Physical Geography, Eötvös University, Budapest, Hungary, 1117 Budapest, Pázmány Péter sétány 1/C. E-Mail: telbisztom@caesar. elte.hu – G. Kovács, Department of Geophysics and Space Sciences, Eötvös University, Budapest – B. Székely, Research Groups Photogrammetry and Remote Sensing, Department of Geodesy and Geoinformation, Vienna University of Technology, Vienna, Austria, and Department of Geophysics and Space Sciences, Eötvös University, Budapest J. Szabó, Department of Physical Geography, Eötvös University, Budapest.